CryoTEMPO-EOLIS

Elevation Over Land Ice from Swath Algorithm Theoretical Basis Document

Land Ice Elevation Thematic Point Product

Land Ice Elevation Thematic Gridded Product

Issue: 2.3

Date: 13th May 2024

Approval

Name	Date	Signed
Alessandro Di Bella ESA		Alessandro Di Bella Digitally signed by Alessandro Di Bella Date: 2024.07.13 13:08:40 +02'00'
Noel Gourmelen University of Edinburgh		
Livia Jakob Earthwave	13th June 2024	Ljakob

Document Versions

Issue	Date	Reason for change
1.0	8th November 2021	First version of document
1.1	29th December 2021	Updated and reviewed
2.0	5th September 2022	Updated for CryoTEMPO EOLIS Baseline 2
2.1	15th March 2023	Updated for release of CryoTEMPO-EOLIS Baseline 2
2.2	22nd January 2024	Updated for the release of new products
2.3	13th May 2024	Updated to include the new Antarctic Ice Shelves product

Contents

List of acronyms

DEM	Digital Elevation Model
EO	Earth Observation
EOLIS	Elevation Over Land Ice from Swath
ESA	European Space Agency
FTP	File Transfer Protocol
GDAL	Geospatial Data Abstraction Library
GS	Ground Segment
LRM	Low Resolution Mode
NetCDF	Network Common Data Form (binary file format)
OIB	Operation Ice Bridge
PDGS	Payload Download Ground Segment
POCA	Point-Of-Closest-Approach
SARIn	Synthetic Aperture Radar Interferometric
STSE	Support To Science Element
UoE	University of Edinburgh
UTC	Coordinated Universal Time
XML	Extensible Mark-up Language

1. Introduction

1.1 Purpose and Scope

This document contains the Algorithm Theoretical Basis for the ESA CryoTEMPO-EOLIS project. The ATBD describes the scientific background and principle of the algorithms, their expected or known accuracy and performance, the input and output data, as well as capabilities and limitations. The CryoTEMPO-EOLIS consists of two distinct products:

1) a point product containing elevation point measurements with an associated uncertainty;
2) a gridded product containing a spatial interpolation of the point product onto a uniform grid of elevations and corresponding uncertainty.

This product covers the two ice sheets (Antarctic Ice Sheet and Greenland Ice Sheet) as defined by Rignot et al. (2011), in accordance with IMBIE (The IMBIE Team, 2018; The IMBIE Team, 2020), the Antarctic Ice Shelves as defined by MEaSUREs BedMachine V3 (Morlighem M. , 2022; Morlighem et al., 2020) and the glacier regions, as defined by RGI 7.0 (RGI 7.0 Consortium, 2023). The glacier regions include Iceland, Svalbard, Arctic Canada, Russian Arctic, Alaska, Southern Andes, High Mountain Asia, Western Canada & USA, Scandinavia, Central Europe, Low Latitudes, New Zealand, the peripheral glaciers in Antarctica and the peripheral glaciers in Greenland.

1.2 Reference Websites

CryoTEMPO-EOLIS Project Website: http://cryotempo-eolis.org/

CryoTOP Evolution: https://cryotop-evolution.org/

CryoSat + Mountain Glaciers: http://www.cryosat-mtg.org/

ESA CryoSat-2 Data Download: https://science-pds.cryosat.esa.int/

Operation IceBridge: https://nsidc.org/data/icebridge/

Arctic DEM: https://www.pgc.umn.edu/data/arcticdem/

REMA DEM: https://www.pgc.umn.edu/data/rema/

Gapless-REMA100: https://figshare.com/articles/dataset/Gapless-REMA100/19122212

SRTM DEM: https://srtm.csi.cgiar.org/

Copernicus DEM: https://registry.opendata.aws/copernicus-dem

ICESat-2: https://icesat-2.gsfc.nasa.gov/

Randolph Glacier Inventory (RGI) 7.0: https://glims-rgi.github.io/rgi_user_guide/welcome.html

MEaSUREs BedMachine: https://nsidc.org/data/nsidc-0756/versions/3

Polar+Iceshelves: https://polar-iceshelf.org

2. Scientific Background

Global ice loss has been increasing over the past decades, with large contributions from glaciers, as well as from the two ice sheets (Slater et al., 2021). Global and continuous monitoring of these environments however remains a challenging task with estimates relying on a variety of observations and models to achieve the required spatial and temporal coverage.

CryoSat-2 is the first altimeter to carry a SAR interferometer, which allows a sharper footprint and the ability to precisely locate the position of the ground echo (Wingham et al., 2004). In practice, CryoSat's revolutionary interferometric design has allowed several technical breakthroughs and led to the application of radar altimetry to environments that were previously unforeseen. The conventional method of processing CryoSat-2 waveforms measures surface elevations at the Point-Of-Closest-Approach (POCA), sampling one elevation measurement per waveform at the closest point on the Earth's surface beneath the satellite. In contrast, the novel swath processing technique extracts multiple elevation measurements across the waveform, increasing the data volume and improving spatial as well as temporal coverage, enabling the use of CryoSat-2 measurements in new environments such as on mountain glaciers (Gourmelen et al., 2018).

Following on from the early demonstration of the technique and its potential impact, the "CryoSat ThEMatic PrOducts – SWATH Cryo-TEMPO" project (CryoTEMPO-EOLIS) consolidates the research and development undertaken during the CryoSat+ CryoTop / CryoTop evolution ESA STSE projects (Gourmelen et al., 2018), the CryoSat+ Mountain Glaciers project (Foresta et al., 2016; Foresta et al., 2018; Jakob L. et al., 2021; Jakob & Gourmelen, 2023) and Polar+ Ice Shelves project (Gourmelen et al., 2017; Davison et al., 2023) into operational products. The purpose of the thematic products is to make the data available to the wider scientific community in a form that does not require a detailed understanding of the sensor used and extensive processing. This product allows users to perform analysis using swath data, and provides an uncertainty metric on which to filter the data to a desired precision.

3. Processing

The processing chain to generate the thematic products consists of multiple phases. The diagram below illustrates the sequence of steps in the processing chain.

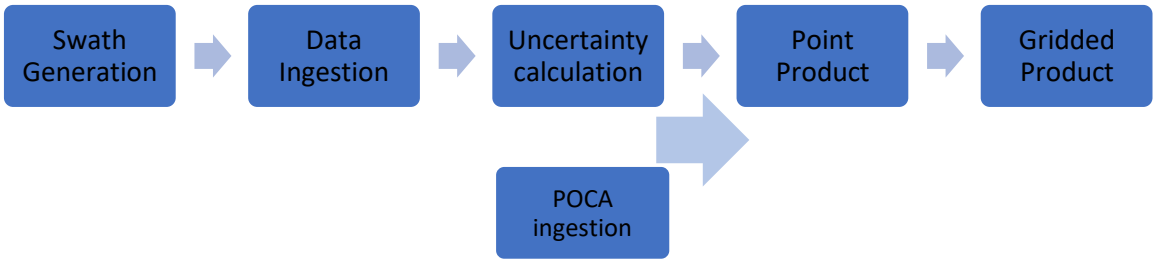

Figure 1: Processing Chain Sequence.

The swath generation as described in (Gourmelen et al., 2018) uses the along track L1B files and a reference DEM to compute a set of points perpendicular to the satellite's track referred to as the

swath points. The data ingestion phase builds a spatial and temporal index of the along track data into 100 x 100 km tiles. The uncertainty value for a given point of data is computed using these tiles.

The Level 2 Baseline D NetCDF feed is used to source the POCA data that is ingested and used to create the point and gridded products. The columns used are: *height_1_20_ku* for the elevations, *retracker_1_quality_20_ku* for retracker quality filtering*, lat_poca_20_ku* and *lon_poca_20_ku* for position. The ESA CryoSat Product Handbook contains definitions of the column names (ESA, 2019).

The latitude and longitude coordinates are transformed to a local coordinate system using a consistent projection with the swath point data (see Table 1). The difference of POCA elevation to the reference DEM is used as a filter for erroneous data excluding any POCA points that are greater than 100m in difference from a reference DEM. The POCA data is also filtered on *retracker_1_quality_20_ku,* excluding points with a retracker quality metric equal to 0. These points are excluded because they correspond to locations where the retracker has failed, and the point position that has been recorded has defaulted to nadir.

4. Point Product

The CryoTEMPO-EOLIS point product is a set of high quality CryoSat-2 swath altimetry point data with uncertainty metrics applied. This product is designed to be user-friendly, so that it can be used by non-altimetry experts. The point products cover the following regions: Antarctic and Greenland Ice Sheets and peripheral glaciers, Antarctic Ice Shelves, as well as the ice caps and glaciers in Iceland, Svalbard, Alaska, Arctic Canada, Russian Arctic, Southern Andes, High Mountain Asia, Western Canada & USA, Scandinavia, Central Europe, Low Latitudes and New Zealand. The definition of these regions follows the IMBIE definition of the Greenland and Antarctic Ice sheet, the MEaSUREs BedMachine definition of the Antarctic Ice Shelves, and the RGI 7.0 definition of the glacier areas.

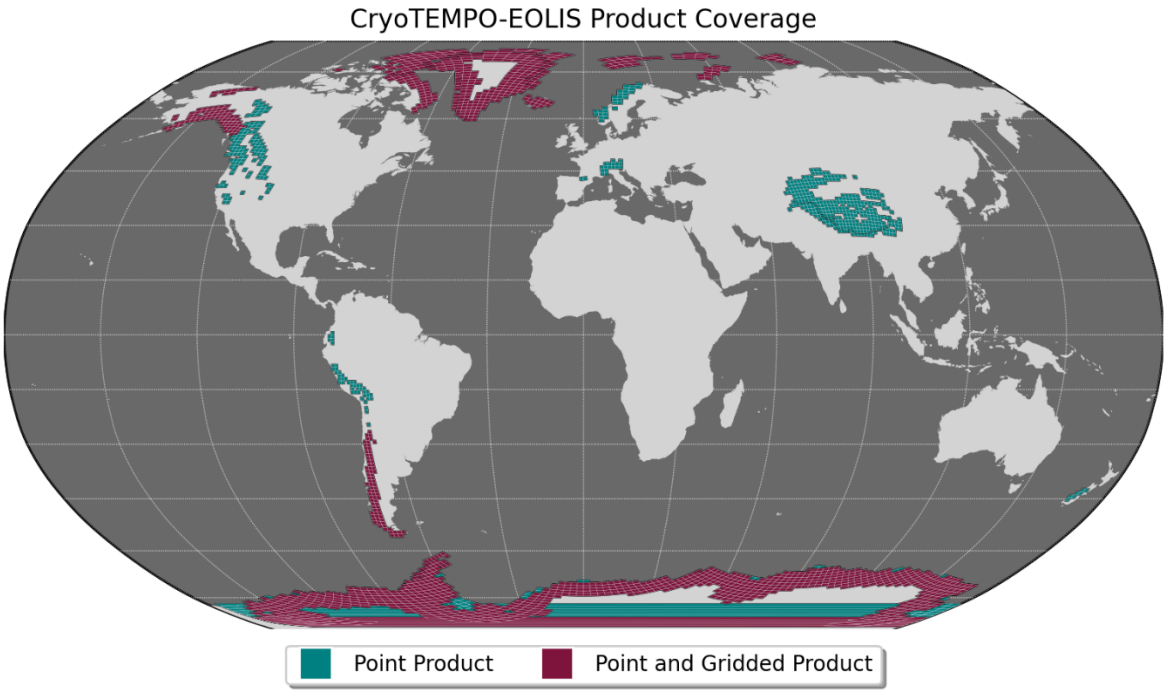

Figure 2: CryoTEMPO-EOLIS product coverage illustrated using grid cells of 100km resolution.

4.1 Point Product Algorithm Description

4.1.1 Swath Processing

Swath processing of CryoSat-2 data has been detailed as part of the CryoSat+ CryoTop / CryoTop evolution ESA STSE projects (Gourmelen et al., 2018).

4.1.2 Phase Model Adjustment

Due to CryoSat-2's slight mis-pointing, the conversion from interferometric phase to angle of arrival is complex and leads to systematic errors in the angle of arrival (Wingham et al., 2004; Recchia et al., 2017). These errors are a function of surface slope, roll angle and distance from POCA. This affects predominantly areas of low surface slopes and leads to artefacts in the EOLIS elevation products (Figure 3).

Ice Sheets

We mitigate this effect using a simple empirical model applied on a waveform basis to the elevation difference between swath and a reference DEM, taking advantage of the systematic nature of the error. For this, the swath waveforms are split into two sections: the *leading edge*, and *non-leading edge*. The *leading-edge* section begins at the POCA and continues until the return signal power peaks. The *non-leading edge* begins at the trailing edge until the end of the swath waveform. A robust linear model is fit to the data within the *leading-edge* section, and a two-part piecewise linear model fit to data within the *non-leading edge*. The model is then applied to the original swath data, ensuring that the mean elevation difference between swath and the reference model is maintained. Underlying topography is considered when applying the adjustment such that only very flat areas with low slope are adjusted. The degree of improvement of the model is also measured to

determine if the adjustment should be applied. This approach works well to greatly reduced features present in the product, with only minor residuals remaining (Figure 3).

Ice Shelves

For the Antarctic Ice Shelves, a physics-driven correction is used to mitigate the systematic errors, for this purpose a dedicated phase correction plugin was developed by Aresys (Recchia et al., 2017).

Glaciers

No correction is necessary for the glacier regions, as they typically have higher slopes and more complex topography.

4.1.3 Tide Correction

Tide correction with CATS2008: a tide correction is applied to the Swath processed data, using the Circum-Antarctic Tidal Simulation Model (CATS2008; Padman et al. (2002), Padman et al. (2008)). The CATS2008 tide model is used to calculate tidal heights at a specific point in space and time. The elevation variations observed by the EOLIS point data due to tidal changes are then corrected by subtracting the tidal elevation from the EOLIS point data.

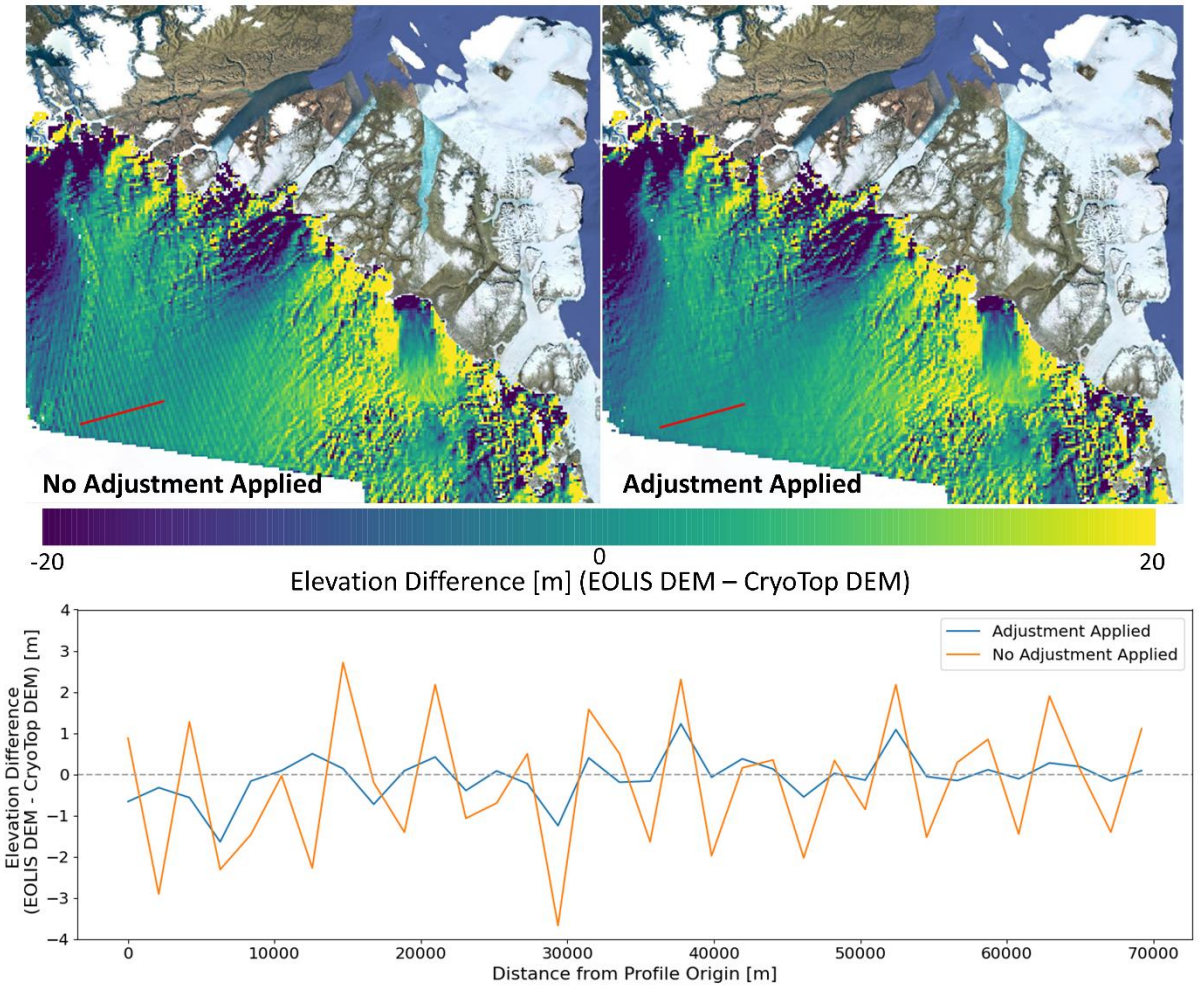

Figure 3: Example of improvement of phase model features in north Greenland. Top: elevation difference between the CryoTEMPO-EOLIS Greenland ice sheet gridded product for February 2019 and the CryoTop Greenland gridded DEM (Gourmelen et al., 2018) before (left) and after (right) the adjustment is applied. Bottom: elevation difference profile over the red line marked in the spatial plot (top), showing the reduction in amplitude of features after the adjustment is applied.

4.1.4 Point Product Uncertainty Score

For each swath elevation measurement an uncertainty value is calculated using a binning approach with several variables associated with measurement quality. This provides a simple metric on which the data can be filtered to a desired precision. This section outlines the elevation uncertainty algorithm.

Firstly, for each region, the swath data is compared to a reference elevation dataset (see Section 4.2.4 for details):

$$\Delta E = E_{swath} - E_{ref}$$

where E_{swath} and E_{ref} are the swath and reference elevations respectively joined within a 10-day time window and 50m radius. A slope correction is applied to ΔE to minimise errors due to variation in topography within the 50m joined distance. The differences, ΔE, are made up of errors in swath dataset, errors in the reference dataset, signal penetration differences between $E_{swath}$and E_{ref}, errors due to variation in elevation within the 10-days period, errors in the slope correction of the 50m joined criteria, as well as other systematic differences. Consequently, it cannot directly be used as a measure of data uncertainty.

A binning approach is then used to calculate standard deviations of the elevation differences ΔE using bins of six different variables, known to impact swath uncertainty (Table 1).

Table 1: Swath point data variables used for elevation uncertainty calibration.

Power in Decibels	As defined in the CryoSat-2 Product Handbook (ESA, 2019)
Coherence	As defined in the CryoSat-2 Product Handbook (ESA, 2019)
Distance to POCA	Distance in metres between the Swath observation and the POCA derived using the TFRMA retracker (Helm et al., 2014)
Along Track Slope	Slope is calculated along the track at a length scale of 400m (the along track resolution stated in ESA CryoSat-2 Product Handbook (ESA, 2019)). Along track slope is defined as change in elevation in metres between 200m in front and 200m behind the observation divided by 400m.
Across Track Slope	Slope is calculated across the track at a length scale of 1600m (the across track pulse limited footprint stated in ESA CryoSat-2 Product Handbook (ESA, 2019)). Across track slope is defined as change in elevation in metres between 800m to the left and 800m to the right of the observation divided by 1600m.
Roughness	Calculated from the reference DEM using the GDAL library function “gdaldem roughness”.

A six-dimensional cube consisting of each variable binned into 6 equal volume bins is generated. The data is sampled using every bin combination across all variables resulting in 6^6 (= 46,656) "quality bins". The quality bins are calculated separately for Antarctic Ice Sheet, Antarctic Ice Shelves, Greenland Ice Sheet and the glacier regions. The latter are split into three groups: RGI regions A, B and C, defined in the Section 4.2.1. For the RGI regions B and C, the *Distance to POCA* variable was removed as sample data size for the uncertainty calculation was not sufficiently large enough.

The standard deviation is calculated from the binned sampled data which gives a range of high to low quality combinations of variables. To ensure that the sample size in each bin is considered, the upper bound of the confidence interval of the standard deviation is calculated:

$$\sigma \leq s\sqrt{\frac{n-1}{\chi^2_{1-\alpha/2}}}$$

where s is standard deviation of the sample, n is sample size, χ^2 is the Chi-square distribution and α is set to 0.05 to give a one-sided 97.5% confidence interval. This upper estimate of the standard deviation is defined as the uncertainty value for each of the quality bin combinations.

The quality bins are then used as a lookup table, where each individual swath elevation measurement is matched to an uncertainty, given its six variable values (see Table 1). It should be noted that the uncertainty metric provided is not a guarantee that the elevation is accurate to within the uncertainty score given. Moreover, it means that for the test sample data, there is a 97.5% confidence that the true standard deviation of the data will be less than the uncertainty score for a combination of variables. In other words, it is a conservative estimate of the uncertainty for a point but does not guarantee the point is not an outlier.

4.2 Point Product Input Data

4.2.1 Definition of region groupings for uncertainty calculation

EOLIS regions are grouped into five categories, distinguished for the quality filters applied and the uncertainty calibration, described in Sections 4.2.1 and 4.2.2 respectively. These groups are defined as follows (in parenthesis the number of each RGI region):

Region Group Name	**EOLIS Region Names**
Antarctic Ice Sheet	Antarctic Ice Sheet
Greenland Ice Sheet	Greenland Ice Sheet
Antarctic Ice Shelves	Antarctic Ice Shelves
RGI regions A	Alaska (01), Arctic Canada North (03) and South (04), Greenland Periphery (05), Iceland (06), Svalbard (07), Russian Arctic (09), Southern Andes (17) and Antarctic Periphery (19)
RGI regions B	Central/South West/South East Asia (13, 14, 15)
RGI regions C	Western Canada & USA (02), Scandinavia (08), Central Europe (11), Low Latitudes (16) and New Zealand (18)

4.2.2 Input Swath Elevation Data

Before the uncertainty score is calculated, the following baseline filters are applied to the swath elevation data to remove any weak signal and poor-quality data:

- Power in Decibels > -160 dB (Antarctic and Greenland Ice Sheets, Antarctic Ice Shelves, RGI regions A), > -175 dB (RGI regions B and C)
- Power Scaled > 100
- Coherence > 0.6
- Absolute difference to a reference DEM < 100 m
- Median absolute deviation of swath compared to reference DEM < 6 m (Antarctic and Greenland Ice Sheets, Antarctic Ice Shelves), < 10 m (RGI regions A, B and C)

These filters are based on standard filter criteria used in the CryoSat+ CryoTop / CryoTop evolution ESA STSE projects (Gourmelen et al., 2018) and then adapted based on comparisons to reference datasets (such as OIB (Studinger, 2014) and ICESat2 (Smith et al., 2021)) to find values which minimised the standard deviations of the elevation difference whilst also maintaining an optimal volume of points. The minimum power in decibels threshold was lowered for RGI regions B and C to reflect the mean power of the distribution due to high surface slope. For all glacier regions (RGI regions A, B and C), the median absolute deviation of elevation difference was on average observed to be higher, due to the more complex topography compared to Greenland and Antarctic Ice Sheets, and as a result the threshold was raised to 10 m.

4.2.3 Reference DEMs

Different reference DEMs are used in different regions: the Arctic DEM mosaic is used for Greenland, Iceland, Svalbard, Russian Arctic, Arctic Canada and Alaska (Porter et al., 2018), the Gapless-REMA100 DEM is used for Antarctica (Dong et al., 2022), TanDEM-X DEM (German Aerospace Center (DLR), 2018) filled with the SRTM DEM (Jarvis et al., 2008) is used for Southern Andes and High Mountain Asia, and Copernicus GLO-30 (European Space Agency; Sinergise, 2021) is used for all the RGI Regions C.

4.2.4 Uncertainty Calibration Data Sets

ATL06 (ATLAS/ICESat-2 L3A Land Ice Height; Advanced Topographic Laser Altimeter System) data (Smith et al., 2021) is used as a reference data set for all EOLIS regions.

For the quality bins of the RGI Regions B, a combination of all joined data over RGI Regions B and Alaska is used, which is roughly an equal split across both regions. The Alaska data was used to increase data volume for the uncertainty calculation.

For the quality bins of the RGI Regions C, a combination of all joined data over RGI Regions C, B and Alaska is used, in order to increase the data volume and cover approximately all the parameter space.

4.3 Point Product Uncertainty Score Output

The algorithm provides a six-dimensional cube consisting of the six variables binned into six equal volume bins with associated 97.5% upper one-sided confidence bound for each combination (Table

2)or each swath point, the associated variables are matched to the bin definitions and the estimated uncertainty score for that bin is assigned to the swath point.

Table 2: Definition of uncertainty bins for Antarctic Ice Sheet, Greenland Ice Sheet, Antarctic Ice Shelves, RGI regions A, B and C. Each bin is between two bin edges, e.g. 0-1, 1-2 …. 5-6.

Antarctic Ice Sheet

Bin Edge	Power [dB]	Coherence	Roughness	Slope Across	Slope Along	Distance To POCA [m]
0	-160.00	0.600	0.00	-0.3612	-0.4640	0
1	-157.23	0.773	0.87	-0.0105	-0.0070	4130
2	-154.80	0.852	1.43	-0.0050	-0.0024	6413
3	-152.49	0.900	2.17	-0.0020	0.0001	7793
4	-150.04	0.933	3.33	0.0000	0.0027	9314
5	-146.76	0.957	5.43	0.0042	0.0074	11126
6	0.00	1.010	128.20	0.3624	0.2626	22544

Greenland Ice Sheet

Bin Edge	Power [dB]	Coherence	Roughness	Slope Across	Slope Along	Distance To POCA [m]
0	-160.00	0.600	0.00	-0.3492	-0.6794	0
1	-157.09	0.813	1.01	-0.0123	-0.0078	3649
2	-154.52	0.885	1.73	-0.0066	-0.0026	6104
3	-151.98	0.921	2.62	-0.0034	0.0000	7703
4	-149.22	0.946	3.85	-0.0008	0.0028	9387
5	-145.67	0.965	5.93	0.0074	0.0077	11255
6	0.00	1.000	239.80	0.4041	0.5017	22894

Antarctic Ice Shelves

Bin Edge	Power [dB]	Coherence	Roughness	Slope Across	Slope Along	Distance To POCA [m]
0	-160.00	0.600	0.00	-0.1873	-0.3060	0
1	-157.25	0.695	0.24	-0.0006	-0.0009	6058
2	-154.55	0.750	0.32	-0.0002	-0.0003	7473
3	-151.91	0.799	0.40	0.0000	0.0000	8748
4	-149.21	0.856	0.53	0.0002	0.0003	9913
5	-146.00	0.918	0.82	0.0005	0.0008	11058
6	0.00	1.010	118.64	0.3129	0.4281	36638

RGI regions A

Bin Edge	Power [dB]	Coherence	Roughness	Slope Across	Slope Along	Distance to POCA [m]
0	-160.00	0.600	0.00	-0.5013	-0.8264	0
1	-158.14	0.802	3.91	-0.0239	-0.0226	366
2	-156.19	0.881	5.46	-0.0124	-0.0097	1421
3	-154.13	0.923	6.98	-0.0016	0.0002	3103
4	-151.84	0.949	8.87	0.0114	0.0106	5108
5	-148.78	0.969	11.89	0.0240	0.0235	7364
6	0.00	1.000	299.18	0.4724	0.8077	26944

RGI regions B

Bin Edge	Power [dB]	Coherence	Roughness	Slope Across	Slope Along
0	-175.00	0.600	0.00	-0.5340	-1.0270
1	-167.70	0.719	6.04	-0.0397	-0.0408
2	-164.91	0.816	10.39	-0.0090	-0.0071
3	-161.74	0.891	16.78	0.0121	0.0144
4	-157.12	0.946	29.90	0.0434	0.0516
5	0.00	1.000	639.62	0.5360	0.9060

RGI regions C

Bin Edge	Power [dB]	Coherence	Roughness	Slope Across	Slope Along
0	-175.00	0.600	0.00	-0.5340	-1.0270
1	-167.68	0.708	4.23	-0.0468	-0.0536
2	-165.18	0.801	7.29	-0.0106	-0.0098
3	-162.43	0.877	12.11	0.0143	0.0168
4	-158.15	0.938	22.46	0.0535	0.0606
5	0.00	1.000	639.62	0.5396	1.0117

4.4 Choice of Uncertainty Score Variables

For each variable used in the uncertainty calculation (see Table 1) there is a clear link between the value of the variable and the uncertainty score (Figure 4).

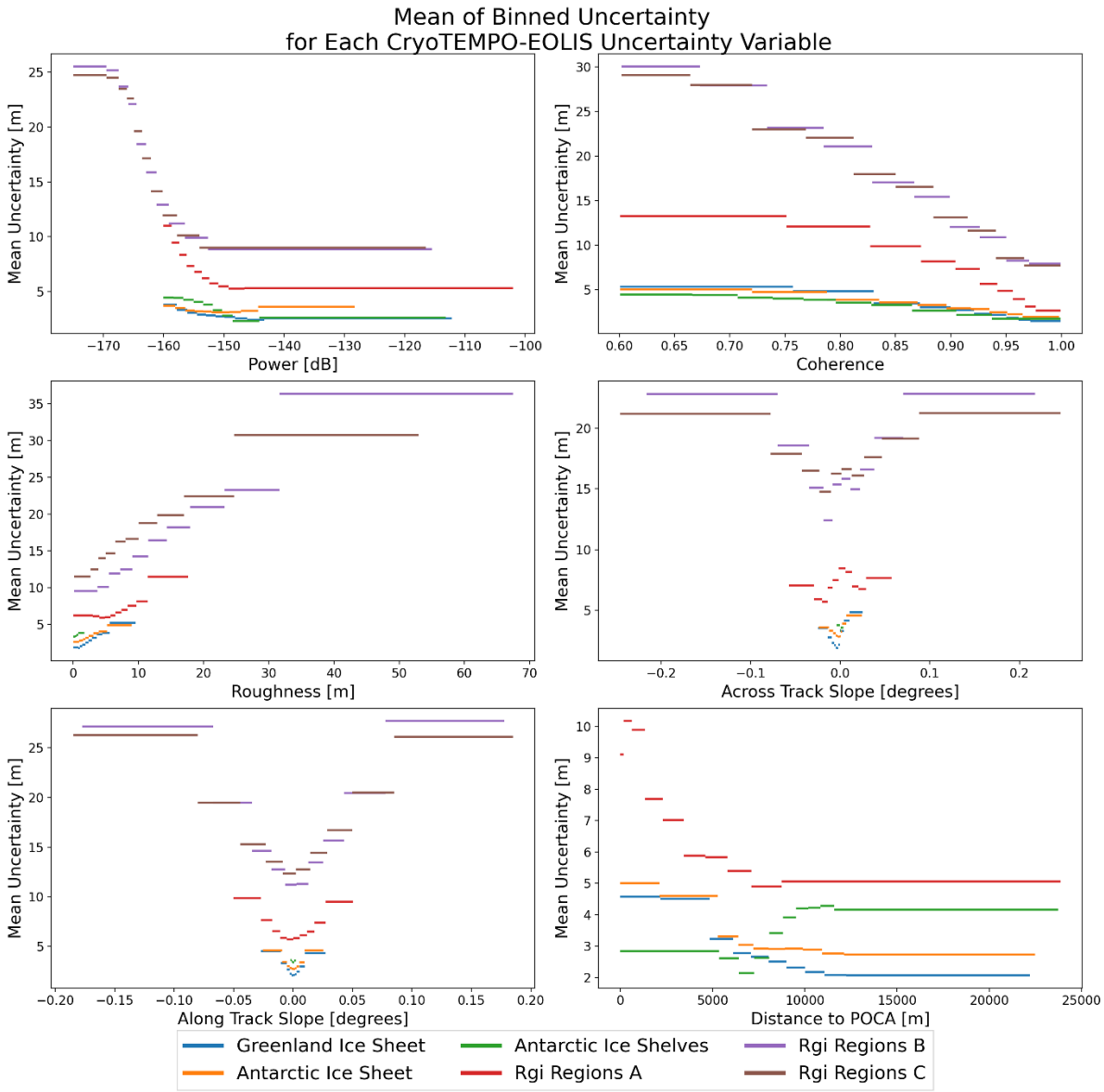

Figure 4: Comparison of uncertainty calculated using equal volume bins of points for each variable for Greenland Ice Sheet (blue), Antarctic Ice Sheet (orange), Antarctic Ice Shelves (green), RGI regions A (red), RGI regions B (purple) and RGI regions C (brown). Uncertainty variables presented in this figure are defined in Table 1.

Note that Figure 4 illustrates the relationship between uncertainty and each individual variable as a comparison exercise, however the uncertainty calculation is a combination of all variables and thus is a six-dimensional relationship (or five-dimensional for the region groups that do not make use of *Distance to POCA*). Higher slope of the underlying terrain results in a higher uncertainty score: this is observed for *Along Track Slope* and A*cross Track Slope*. Swath data with high power in decibels results in a lower uncertainty score, with the opposite applying for low power data points. Similar linear correlations are observed for coherence where high coherence data has a low uncertainty

score and low coherence data has a higher uncertainty score. The same relationship is recorded for the distance to the nearest POCA point, with swath points further from the POCA having a low uncertainty score. Finally, we see that data with low roughness, a measure of the irregularity of the surface, has a low associated uncertainty score, and higher roughness results in higher uncertainties.

5. Gridded Product

The CryoTEMPO-EOLIS gridded products are monthly DEMs that provide users with instant access to gridded and averaged point data at 2km spatial resolution. The CryoTEMPO-EOLIS DEMs are a valuable tool to monitor changes in topography at monthly temporal resolution. Gridded products are published for the following regions:

- Greenland Ice Sheet
- Antarctic Ice Sheet
- Alaska
- Arctic Canada North
- Arctic Canada South
- Greenland periphery
- Iceland
- Svalbard
- Russian Arctic
- Southern Andes
- Antarctic periphery

5.1 Gridding Algorithm Description

The gridded products are generated on a monthly basis, using the CryoTEMPO-EOLIS point product data, with each monthly DEM using a 3-month overlapping temporal window which is centred on the middle of the publication month. The gridding method uses the methods proposed by Jakob et al. (2021) to handle complex topography in the glacier regions.

There are multiple phases in the construction of the gridded product from the point data, which are detailed below:

1) **Topography removal:** topography is removed from the gridding by subtracting the reference DEM from the swath elevation measurements at a point level (hereinafter referred to as *DEM difference*).
2) **Median calculation:** for each 2km posting, all *DEM difference* values within a 2km radius are combined using a median calculation to create a gridded *DEM difference*.
3) **Reduction of boundary noise and artefacts:** a median filter is applied iteratively 2 times to the gridded *DEM difference* values.
4) **Topography retrieval:** the gridded *DEM difference* values are converted back to a DEM using the reference DEM.

5.2 Gridded Product Input Data

For both the Greenland and Antarctic Ice Sheets, the gridded product uses swath data points that have a maximum uncertainty of 7m as a quality filter. For all other regions, the gridded product uses swath data points that have a maximum uncertainty of 20m as a quality filter. This is consistent with the maximum uncertainty filters applied to the point products.

5.3 Gridded Product Uncertainty Score

5.3.1 Uncertainty Propagation and Spatial Auto-Correlation

The point uncertainty is propagated to a gridded uncertainty, taking spatial auto-correlation into account. An uncertainty estimate is provided for each pixel using the following equation:

$$\sigma_p = \sqrt{\sum_{i}^{n} \frac{1}{n^2}\sigma_i^2 + \sum_{i}^{n}\sum_{j(j\neq i)}^{n} \frac{1}{n^2}\rho_{ij}\sigma_i\sigma_j}$$

where:

σ_p = Uncertainty of a pixel

σ_i, σ_j = Uncertainty of individual points

ρ_{ij} = Spatial auto-correlation between 2 points

n = Number of points contributing to a pixel

This equation reduces to the standard error of the mean uncertainty if all points have 0 correlation. Conversely, if all points are 100% correlated, the uncertainty is the mean of the uncertainties, which is a maximum of 20m given the maximum uncertainty of a point is 20m.

A semi-variogram is used to determine the spatial auto-correlation ρ_{ij} based on the separation of the points. This semi-variogram is calculated using the Python SciKit Gstat library.

For each region a sample of 50,000 is used to derive semi-variograms with: a maximum lag of 5km, an even binning function, the *stable model* and the *Cressie estimator*. Using the sill as an estimate for the covariance and the derived semi-variance, the estimated spatial auto-correlation as a function of distance between points is then calculated as:

$$\rho_{dist} = \frac{Sill - SV_{dist}}{Sill}$$

where:

ρ_{dist} = spatial auto-correlation for a given distance

SV_{dist} = Semi-variance for a given distance

A third order polynomial is then fit to the ρ_{dist} values between 0 and 5km to give an equation that can be used to estimate the spatial auto-correlation.

$$\rho(x) = ax^3 + bx^2 + cx + d$$

where x is the distance between observations. The calculated coefficients are provided in Table 3.

Table 3: Spatial auto-correlation coefficients for the gridded product regions.

Region Name	a	b	c	d
Greenland Ice Sheet	-1.5253e-11	1.5099e-7	-0.0005	0.5994
Antarctic Ice Sheet	-1.4327e-11	1.3909e-7	-0.0004	0.4910
Alaska	-7.6986e-12	9.2200e-8	-0.0004	0.5920
Arctic Canada North	-9.6405e-12	1.0856e-7	-0.0004	0.4150
Arctic Canada South	-8.8506e-12	1.0059e-7	-0.0004	0.4140
Greenland Periphery	-8.6387e-12	9.6853e-8	-0.0003	0.3636
Iceland	-7.6986e-12	9.2200e-8	-0.0004	0.5912
Svalbard	-8.2889e-12	9.3604e-8	-0.0003	0.3712
Russian Arctic	-6.2968e-12	7.4029e-8	-0.0003	0.4576
Southern Andes	-8.1924e-12	9.8736e-8	-0.0004	0.6460
Antarctic Periphery	-6.2600e-12	7.9273e-8	-0.0003	0.6092

Figure 5 shows an example of the spatial autocorrelation as a function of distance, for the Vatnajökull ice cap. This figure shows that for the applicable distance of 4000 m, the auto-correlation is small, and has a maximum of 0.49 when the distance is 0 m. This is expected as two independent observations at the same location will not be identical due to other uncertainties within the signal.

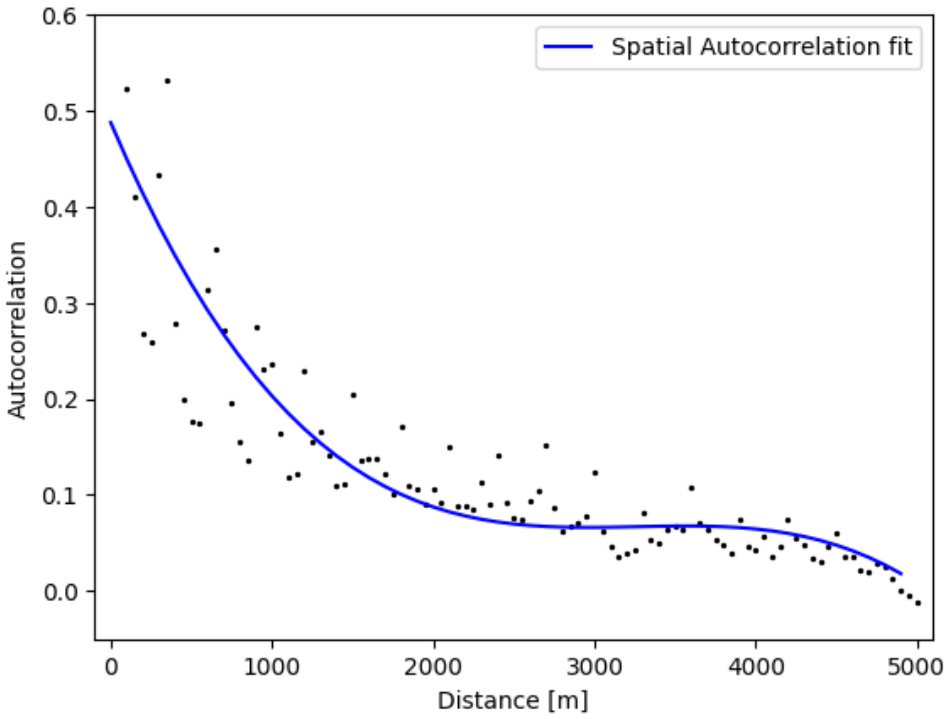

Figure 5: Spatial auto-correlation vs distance for the Vatnajökull ice cap.

Using the spatial auto-correlation, $\rho(x)$, the uncertainty formula shown previously means that in general, low pixel uncertainties of order 1-2 m are seen when there is a high volume of widely distributed points contributing to a pixel. Conversely much higher uncertainties are observed when there is a low volume of points or narrowly distributed points.

This can be demonstrated by looking at a pixel over time, as shown in Figure *6*. Outliers are clearly seen and highlighted by the uncertainty calculation.

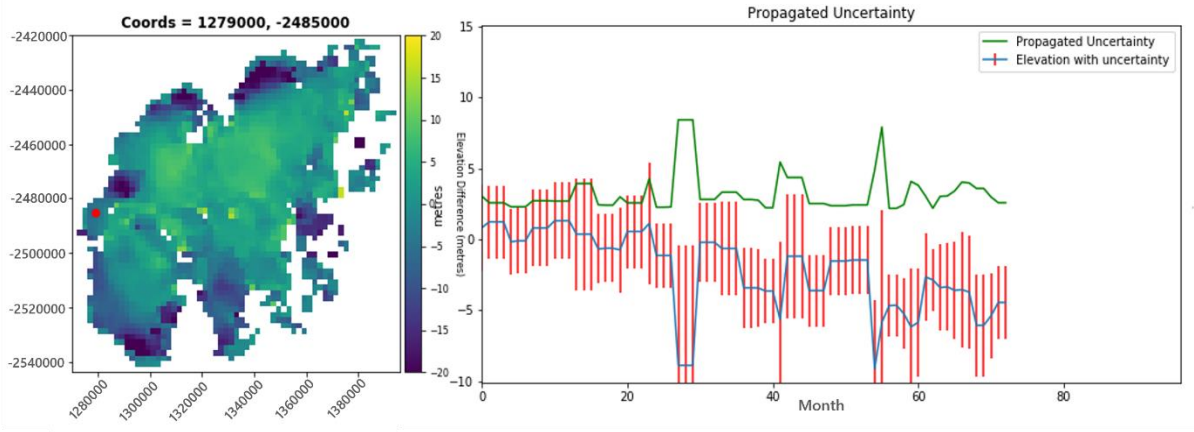

Figure 6: Example pixel near the edge of the Vatnajökull ice cap. Outlier values are showing a higher uncertainty.

5.3.2 Pre-Clustering

To improve computing performance the following intermediate step is used to the calculation of the propagated gridded uncertainty. All points within a specified distance (the pre-clustering radius) are pre-clustered and an effective uncertainty is calculated, assuming that they are all 100% spatially correlated. The reduced dataset is then propagated following the correlation model described in the previous section. This is motivated by the fact that points close to each other are indeed highly (>60%) correlated, and allows faster computation while maintaining a high level of accuracy. For the Greenland and Antarctic ice sheets, a pre-clustering radius of 100m is used. For all other gridded regions, a pre-clustering radius of 50m is used.

6. References

Davison, B., Hogg, A., Gourmelen, N., Jakob, N., Wuite, J., Nagler, T., . . . Engdahl, M. (2023). Annual mass budget of Antarctic ice shelves from 1997 to 2021. *Science Advances, 9*(41). https://doi.org/https://doi.org/10.1126/sciadv.adi0186

Dong, Y., Zhao, J., Caiyong, L., & Liao, M. (2022). Gapless-REMA100: A gapless 100-m Reference Elevation Model of Antarctica with voids filled by multi-source DEMs. *ISPRS Journal of Photogrammetry and Remote Sensing*.

Dunse, T., Schellenberger, T., Hagen, J. O., Kääb, A., Schuler, T. V., & Reijmer, C. H. (2015). Glacier-surge mechanisms promoted by a hydro-thermodynamic feedback to summer melt. *The Cryosphere, 9*(1), 197-215. https://doi.org/10.5194/tc-9-197-2015

ESA. (2019). *CryoSat Baseline D Product Handbook.* Retrieved from https://earth.esa.int/documents/10174/125272/CryoSat-Baseline-D-Product-Handbook

European Space Agency; Sinergise. (2021). Copernicus Global Digital Elevation Model. Retrieved 9 1, 2023, from https://registry.opendata.aws/copernicus-dem

Foresta, L., Gourmelen, N., Pálsson, F., Nienow, P., Björnsson, H., & Shepherd, A. (2016). Surface elevation change and mass balance of Icelandic ice caps derived from swath mode CryoSat-2 altimetry. *Geophysical Research Letters, 43*(12), 138-145. https://doi.org/10.1002/2016GL071485

Foresta, L., Gourmelen, N., Weissgerber, F., Nienow, P., Williams, J. J., Shepherd, A., . . . Plummer, S. (2018). Heterogeneous and rapid ice loss over the Patagonian Ice Fields revealed by CryoSat-2 swath radar altimetry. *Remote Sensing of Environment, 211*, 441-455. https://doi.org/10.1016/j.rse.2018.03.041

German Aerospace Center (DLR). (2018). TanDEM-X - Digital Elevation Model (DEM) - Global, 90m. https://doi.org/10.15489/ju28hc7pui09

Gourmelen, N., Escorihuela, M. J., Shepherd, A., Foresta, L., Muir, A., Garcia-Mondéjar, A., . . . Drinkwater, M. R. (2018). CryoSat-2 swath interferometric altimetry for mapping ice elevation and elevation change. *Advances in Space Research, 62*(6), 1226-1242. https://doi.org/10.1016/j.asr.2017.11.014

Gourmelen, N., Goldberg, D., Snow, K., Henley, S., Bingham, R., Kimura, S., . . . Jan van de Berg, W. (2017). Channelized Melting Drives Thinning Under a Rapidly Melting Antarctic Ice Shelf. *AGU, 44*(19), 9796-9804. https://doi.org/https://doi.org/10.1002/2017GL074929

Helm, V., Humbert, A., & Miller, H. (2014). Elevation and elevation change of Greenland. *Cryosphere, 8*(4), 1539-1559. https://doi.org/10.5194/tc-8-1539-2014

Hugonnet, R., McNabb, R., Berthier, E., Menounos, B., Nuth., C., Girod, L., . . . Kääb, A. (2021). Accelerated global glacier mass loss in the early twenty-first century. *Nature, 592*, 726–731. https://doi.org/10.1038/s41586-021-03436-z

Jakob, L., & Gourmelen, N. (2023). Glacier Mass Loss Between 2010 and 2020 Dominated by Atmospheric Forcing. *Geophysical Reseach Letters , 50*(8), 1-10. https://doi.org/https://doi.org/10.1029/2023GL102954

Jakob, L., & Gourmelen, N. (2023). Glacier Mass Loss Between 2010 and 2020 Dominated by Atmospheric Forcing. *Geophysical Research Letters, 50*(8), 1-10. https://doi.org/10.1029/2023GL102954

Jakob, L., Gourmelen, N., Ewart, M., & Plummer, S. (2021). Spatially and temporally resolved ice loss in High Mountain Asia and the Gulf of Alaska observed by CryoSat-2 swath altimetry between 2010 and 2019. *The Cryosphere, 15*(4), 1845-1862. https://doi.org/10.5194/tc-15-1845-2021

Jarvis, A., Reuter, H. I., Nelson, A., & Guevara, E. (2008). *'Hole-filled seamless SRTM data V4', International Centre for Tropical Agriculture (CIAT), available from https://srtm.csi.cgiar.org.*

McMillan, M., Shepherd, A., Gourmelen, N., Dehecq, A., Leeson, A., Leeson, A., . . . Strozzi, T. (2014). Rapid dynamic activation of a marine-based Arctic ice cap. *Geophysical Research Letters, 41*, 8902– 8909. https://doi.org/10.1002/2014GL062255

Morlighem, M. (2022). MEaSUREs BedMachine Antarctica, Version 3. *MEaSUREs BedMachine Antarctica, Version 3*. Boulder, Colorado, USA: NASA National Snow and Ice Data Center Distributed Active Archive Center. https://doi.org/https://doi.org/10.5067/FPSU0V1MWUB6

Morlighem, M. E., Rignot, T., Binder, D. D., Blankenship, R., Drews, G., & Eagles, O. (2020). Deep glacial troughs and stabilizing ridges unveiled beneath the margins of the Antarctic ice sheet. *Nature Geoscience, 13*, 132-137. https://doi.org/https://doi.org/10.1038/s41561-019-0510-8

Padman, L., Erofeeva, S., & Fricker, H. (2008). Improving Antarctic tide models by assimilation of ICESat laser altimetry over ice shelves. *Geophysical Research Letters, 35*. https://doi.org/http://dx.doi.org/10.1029/2008GL035592

Padman, L., Fricker, H. A., Coleman, R., Howard, S., & Erofeeva, L. (2002). A new tide model for the Antarctic ice shelves and seas. *Annals of Glaciology, 34*, 247-254. https://doi.org/doi:10.3189/172756402781817752

Porter, C., Morin, P., Howat, I., Noh, M.-J., Bates, B., Peterman, K., . . . Nakamura, H. (2018). ArcticDEM, Version 3. *Harvard Dataverse*. https://doi.org/10.7910/DVN/OHHUKH

Recchia, L., Scagliola, M., Giudici, D., & Kuschnerus, M. (2017). An Accurate Semianalytical Waveform Model for Mispointed SAR Interferometric Altimeters. *IEEE Geoscience and Remote Sensing Letter, 14*, 1537-1541.

RGI 7.0 Consortium. (2023). Randolph Glacier Inventory - A Dataset of Global Glacier Outlines, Version 7.0. Boulder, Colorado, USA: NSIDC: National Snow and Ice Data Center. https://doi.org/doi:10.5067/f6jmovy5navz

RGI Consortium. (2017). Randolph Glacier Inventory - A Dataset of Global Glacier Outlines, Version 6. *NSIDC: National Snow and Ice Data Center*. https://doi.org/10.7265/4m1f-gd79

Rignot, E., Velicogna, I., van den Broeke, M. R., Monaghan, A., & Lenaerts, J. T. (2011). Acceleration of the contribution of the Greenland and Antarctic ice sheets to sea level rise. *Geophysical Research Letters, 38*. https://doi.org/10.1029/2011GL046583

Slater, T., Lawrence, I. R., Otosaka, I. N., Shepherd, A., Gourmelen, N., Jakob, L., . . . Nienow, P. (2021). Review article: Earth's ice imbalance. *The Cryosphere*, 233–246.

Smith, B., Adusumulli, S., Csathó, B. M., Felikson, D., Fricker, H. A., Gardner, A., . . . ICESAT-2 Science Team. (2021). ATLAS/ICESat-2 L3A Land Ice Height, Version 5. *NASA National Snow and Ice Data Center Distributed Active Archive Center*. https://doi.org/10.5067/ATLAS/ATL06.005

Studinger, M. (2014). IceBridge ATM L2 Icessn Elevation, Slope, and Roughness, Version 2. *NASA National Snow and Ice Data Center Distributed Active Archive Center*. https://doi.org/10.5067/CPRXXK3F39RV

The IMBIE Team. (2018). Mass balance of the Antarctic ice sheet from 1992 to 2017. *Nature, 558*(7709), 219-222. https://doi.org/10.1038/s41586-018-0179-y

The IMBIE Team. (2020). Mass balance of the Greenland Ice Sheet from 1992 to 2018. *Nature, 579*(7793), 233–239. https://doi.org/10.1038/s41586-019-1855-2

Wingham, D., Phalippou, L., Mavrocordatos, C., & Wallis, D. (2004). The mean echo and echo cross product from a beamforming interferometric altimeter and their application to elevation measuremen. *IEEE Transactions on Geoscience and Remote Sensing, 40*(10), 2305-2323. https://doi.org/10.1109/TGRS.2004.834352

Wouters, B., Gardner, A. S., & Moholdt, G. (2019). Global Glacier Mass Loss During the GRACE Satellite Mission (2002-2016). *Frontiers in Earth Science, 7*. https://doi.org/10.3389/feart.2019.00096